

Precision Rosenbluth measurement of the proton elastic form factors

I. A. Qattan,¹ J. Arrington,² R. E. Segel,¹ X. Zheng,² K. Aniol,³ O. K. Baker,⁴ R. Beams,² E. J. Brash,⁵ J. Calarco,⁶ A. Camsonne,⁷ J.-P. Chen,⁸ M. E. Christy,⁴ D. Dutta,⁹ R. Ent,⁸ S. Frullani,¹⁰ D. Gaskell,¹¹ O. Gayou,¹² R. Gilman,^{13,8} C. Glashauser,¹³ K. Hafidi,² J.-O. Hansen,⁸ D. W. Higinbotham,⁸ W. Hinton,¹⁴ R. J. Holt,² G. M. Huber,⁵ H. Ibrahim,¹⁴ L. Jisonna,¹ M. K. Jones,⁸ C. E. Keppel,⁴ E. Kinney,¹¹ G. J. Kumbartzki,¹³ A. Lung,⁸ D. J. Margaziotis,³ K. McCormick,¹³ D. Meekins,⁸ R. Michaels,⁸ P. Monaghan,⁹ P. Moussiegt,¹⁵ L. Pentchev,¹² C. Perdrisat,¹² V. Punjabi,¹⁶ R. Ransome,¹³ J. Reinhold,¹⁷ B. Reitz,⁸ A. Saha,⁸ A. Sarty,¹⁸ E. C. Schulte,² K. Slifer,¹⁹ P. Solvignon,¹⁹ V. Sulkosky,¹² K. Wijesooriya,² and B. Zeidman²

¹Northwestern University, Evanston, Illinois, 60208

²Argonne National Laboratory, Argonne, Illinois, 60439

³California State University, Los Angeles, Los Angeles, California, 90032

⁴Hampton University, Hampton, Virginia, 23668

⁵University of Regina, Regina, Saskatchewan, Canada, S4S 0A2

⁶University of New Hampshire, Durham, New Hampshire, 03824

⁷Université Blaise Pascal Clermont-Ferrand et CNRS/IN2P3 LPC 63, 177 Aubière Cedex, France

⁸Jefferson Laboratory, Newport News, Virginia, 23606

⁹Massachusetts Institute of Technology, Cambridge, Massachusetts, 02139

¹⁰Istituto Nazionale di Fisica Nucleare, Sezione Sanità, 00161 Roma, Italy

¹¹University of Colorado, Boulder, Colorado, 80309

¹²College of William and Mary, Williamsburg, Virginia, 23187

¹³Rutgers, The State University of New Jersey, Piscataway, New Jersey, 08855

¹⁴Old Dominion University, Norfolk, Virginia, 23529

¹⁵Laboratoire de Physique Subatomique et de Cosmologie, F-38026 Grenoble, France

¹⁶Norfolk State University, Norfolk, Virginia, 23529

¹⁷Florida International University, Miami, Florida, 33199

¹⁸Saint Mary's University, Halifax, Nova Scotia, Canada B3H 3C3

¹⁹Temple University, Philadelphia, Pennsylvania, 19122

(Dated: November 26, 2024)

We report the results of a new Rosenbluth measurement of the proton form factors at Q^2 values of 2.64, 3.20 and 4.10 GeV². Cross sections were determined by detecting the recoiling proton in contrast to previous measurements in which the scattered electron was detected. At each Q^2 , relative cross sections were determined to better than 1%. The measurement focussed on the extraction of G_E/G_M which was determined to 4–8% and found to approximate form factor scaling, *i.e.* $\mu_p G_E \approx G_M$. These results are consistent with and much more precise than previous Rosenbluth extractions. However, they are inconsistent with recent polarization transfer measurements of comparable precision, implying a systematic difference between the two techniques.

PACS numbers: 25.30.Bf, 13.40.Gp, 14.20.Dh

Reproducing the structure of the proton is one of the defining problems of QCD. The electromagnetic structure can be expressed in terms of the electric and magnetic form factors, G_E and G_M , which depend only on the 4-momentum transfer squared, Q^2 . They have traditionally been determined utilizing the Rosenbluth formula [1] for elastic e - p scattering:

$$\frac{d\sigma}{d\Omega_e} = \frac{\sigma_{Mott}}{\varepsilon(1+\tau)} [\tau G_M^2(Q^2) + \varepsilon G_E^2(Q^2)], \quad (1)$$

where $\tau = Q^2/4M_p^2$, ε is the longitudinal polarization of the exchanged virtual photon, $\varepsilon^{-1} = 1 + 2(1 + \tau) \tan^2(\theta_e/2)$, M_p is the proton mass, and θ_e is the electron scattering angle. The form factors are related to the spatial distributions of the charge (G_E) and magnetization (G_M) in the proton, and in the non-relativistic limit are simply the Fourier transformations of these distributions.

A Rosenbluth separation is performed by varying the incident electron energy and electron scattering angle to keep Q^2 constant while varying ε . Rosenbluth separations of G_E and G_M have been reported from 1960 to the present day (see Refs. [2, 3] and references therein). Fits to these data yield $\mu_p G_E/G_M \approx 1$ [2, 4], implying similar charge and magnetization distributions. At large Q^2 values, G_M dominates the cross section at all ε values (contributing more than 90% for $Q^2 > 4$ GeV²), and thus while a Rosenbluth separation can yield a precise extraction of G_M , the uncertainty in G_E increases with increasing Q^2 .

The high- Q^2 behavior of the electric form factor can be more precisely determined in polarization transfer experiments, where longitudinally polarized electrons are scattered from unpolarized protons and both transverse and longitudinal polarization are transferred to the struck proton. During the last few years, polarization transfer

experiments have been performed at Jefferson Lab which measured G_E/G_M up to $Q^2 = 5.6 \text{ GeV}^2$ [5, 6]. These measurements show the ratio decreasing with increasing Q^2 in stark contrast to the approximate scaling observed in Rosenbluth measurements.

At high Q^2 , the quoted uncertainties on the polarization transfer results are much smaller than those for the Rosenbluth extractions. This fact, combined with the scatter in the results from different Rosenbluth measurements, led to speculation that the Rosenbluth determinations of G_E were unreliable. While the scatter appears to be the result of incomplete treatment of normalization uncertainties when combining data from different experiments [4], the Rosenbluth technique is still very sensitive to small corrections to the cross section at large Q^2 values. In this letter, we report the results of a new experiment that utilizes an improved Rosenbluth technique to determine the proton form factor ratio G_E/G_M with uncertainties a factor of two to three smaller than all previous Rosenbluth measurements and comparable to the precision of the polarization transfer measurements.

Experiment E01-001 was performed in Hall A at Jefferson Lab. A $70 \mu\text{A}$ electron beam with energies from 1.9 to 4.7 GeV impinged on a 4-cm liquid hydrogen (LH2) target. Protons from elastic $e-p$ scattering were detected in the High Resolution Spectrometer. An aerogel Cerenkov detector was used to eliminate charged pions from the data, and data from a “dummy” target were used to measure the contribution from the aluminum walls of the target. Table I lists the kinematics of the experiment. Detailed descriptions of the spectrometer and beamline instrumentation can be found in Ref. [7].

TABLE I: Kinematics of the experiment.

E_{beam} (GeV)	$Q^2=2.64 \text{ GeV}^2$		$Q^2=3.20 \text{ GeV}^2$		$Q^2=4.10 \text{ GeV}^2$	
	ε	θ_p ($^\circ$)	ε	θ_p ($^\circ$)	ε	θ_p ($^\circ$)
1.912	0.117	12.631	–	–	–	–
2.262	0.356	22.166	0.131	12.525	–	–
2.842	0.597	29.462	0.443	23.395	0.160	12.682
3.772	0.782	35.174	0.696	30.500	0.528	23.666
4.702	0.865	38.261	0.813	34.139	0.709	28.380

Because the fractional contribution of G_E to the cross section is small at large Q^2 , its extraction is highly sensitive to corrections that modify the ε dependence. All previous Rosenbluth separations involved detection of the electron. The rapid variation of the electron cross section with scattering angle means that any rate-dependent corrections to the cross section will have a strong ε dependence. Varying ε also leads to large changes in the momentum of the scattered electron, and so momentum-dependent corrections will affect the extracted value of G_E . Finally, radiative corrections to the cross section also yield significant ε -dependent corrections.

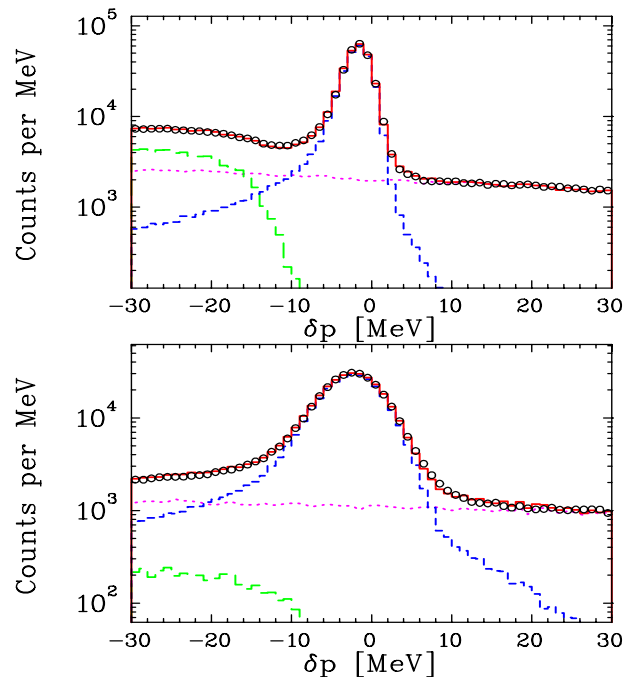


FIG. 1: (Color online) The measured δp spectrum for the low (top) and high (bottom) ε points at $Q^2 = 3.2 \text{ GeV}^2$ (circles). The dotted (magenta) line is the background from the target walls, the long-dash line (green) is the simulated background from $\gamma p \rightarrow \pi^0 p$ and $\gamma p \rightarrow \gamma p$ reactions, the short-dash (blue) line is the simulated elastic spectrum, and the solid (red) line that goes through the data is the sum of the target wall, elastic, and background contributions after each contribution is normalized to the data (see text).

Detecting the struck proton greatly reduces all of these sources of uncertainty. The proton differential cross section ($d\sigma/d\Omega_p$) changes by less than a factor of two over the ε range of the measurement while the electron cross section ($d\sigma/d\Omega_e$) varies by almost two orders of magnitude. In addition, the minimum cross section is twenty times larger for the proton than for the electron. The proton momentum is constant at fixed Q^2 , while the corresponding electron momentum varies by a factor of ten. Additionally, the corrections due to beam energy offsets, scattering angle offsets, and radiative corrections (in particular the electron bremsstrahlung corrections) all have a smaller ε dependence when the proton is detected.

Figure 1 shows the “missing momentum” spectra at two ε values for $Q^2 = 3.20 \text{ GeV}^2$. The missing momentum, δp , is defined as the difference between the measured proton momentum and the proton momentum expected for elastic scattering at the measured proton angle. The δp spectrum is dominated by the $e-p$ elastic peak at $\delta p \approx 0$. To precisely separate elastic scattering from other processes, we need to know the shape of the elastic peak. The peak is simulated using the Monte Carlo code SIMC which takes into account the acceptance and resolution of the spectrometer, energy loss and

multiple scattering of the proton, and radiative corrections [8]. The resolution of the simulation has been modified to reproduce the small non-gaussian tails observed in the data. These are matched to the coincidence data, taken for two beam energies at $Q^2=2.64$ GeV², where the background contributions that dominate the singles spectrum at large $|\delta p|$ values are strongly suppressed. The resolution of the elastic peak is dominated by the angular resolution. The greater width at large ε is due to the increased sensitivity of proton momentum to scattering angle.

Also shown in Fig. 1 is the decomposition of the background into two components. The background that extends to high δp is due to quasielastic scattering and other reactions in the target walls. The other background is mainly due to $\gamma p \rightarrow \pi^0 p$ events, with a small (1–4%) contribution from $\gamma p \rightarrow \gamma p$. The spectrum from these reactions was modeled using a calculated bremsstrahlung spectrum and an s^{-7} cross section dependence. Because of the finite pion mass, the proton spectrum from pion photoproduction cuts off approximately 10 MeV below the elastic peak. For small proton angles, where we have the best resolution, the background from pion photoproduction can be cleanly separated from the elastic protons while at large angles the background becomes small. The correction to the elastic cross section due to contributions from the target walls is approximately 10%, while the inelastic processes from hydrogen contribute less than 2%.

Because the thicknesses are different for the LH2 and dummy targets, the bremsstrahlung yields are also slightly different. We use the dummy data to determine the shape of the endcap contributions, but normalize the contribution to the LH2 spectrum at large δp , where the contribution from the hydrogen is negligible. While the shape of the bremsstrahlung spectrum differs slightly between the dummy and LH2 targets, the effect is only noticeable near the endpoint. The small uncertainty due to the difference in shape is taken into account in the systematic uncertainties.

After removing the background due to the endcaps, the simulated π^0 photoproduction spectra were normalized to the low-momentum sides of the δp spectra (taking into account the elastic radiative tail). Removing this background yields clean spectra of elastic events which are then compared to the elastic simulation. The elastic cross section is taken to be the value used in the simulation, scaled by the ratio of counts in the data to counts in the simulated spectrum.

The proton yield is corrected for deadtime in the data acquisition system (10–20%, measured to better than 0.1%) as well as several other small inefficiencies. Corrections for tracking efficiency, trigger efficiency, and particle identification cuts (using the aerogel Cerenkov detector) were small (<2%) and independent of ε . Finally, we required a single clean cluster of hits in each drift chamber plane to avoid events where the resolution is

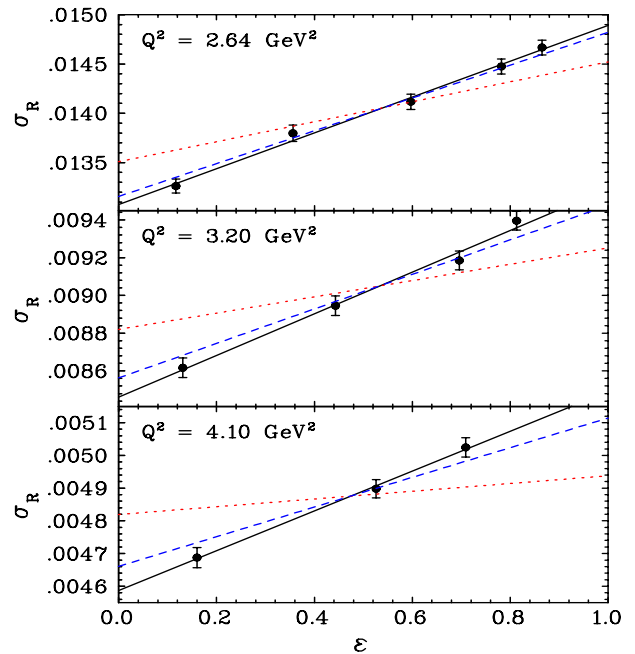


FIG. 2: (Color online) Reduced cross sections as a function of ε . The solid line is a linear fit to the reduced cross section, the dashed line shows the slope predicted from a global analysis of previous Rosenbluth results [9], and the dotted line shows the slope predicted by the polarization transfer experiments [6].

worsened by noise in the chambers. This significantly reduced the non-gaussian tails in the reconstructed quantities, but led to an inefficiency of roughly 7%, with a small (0.25%) ε dependence, possibly related to the small variation of rate with ε . We corrected the yield for the observed inefficiency and applied a 100% uncertainty on the ε -dependence of the correction.

The absolute uncertainty on the extracted cross sections is approximately 3%, dominated by the uncertainty in the angular acceptance (2%), the radiative corrections (1%), corrections for proton absorption in the target and detector stack (1%), the subtraction of endcap and inelastic processes (1%), and the uncertainty in the integrated luminosity (1%). We apply a tight cut on the solid angle, using only the data in the central 1.6 msr of the total ≈ 6 msr acceptance. These tight cuts limit the elastic data to the region of 100% acceptance, but lead to the relatively large uncertainty in the size of the software-defined solid angle. Because the solid angle is identical for all ε values at each Q^2 , this uncertainty affects the absolute cross section, but not the extraction of G_E/G_M .

The largest point-to-point uncertainties, where the error can differ at different ε values, are related to the tracking efficiency (0.2%), uncertainty in the scattering angle (0.2%), the subtraction of the inelastic proton backgrounds (0.2%), and the radiative corrections (0.2%). The total point-to-point systematic uncertainty is 0.45%, and the typical statistical uncertainty varies from 0.25%

at $Q^2 = 2.64 \text{ GeV}^2$ to 0.40% at $Q^2 = 4.1 \text{ GeV}^2$. The cross sections measured at 2.262 GeV have a slight additional uncertainty (0.3%) because these data were taken at lower beam currents (30-50 μA), and so are sensitive to any non-linearity in the beam current measurements and have somewhat different corrections for target heating.

The reduced cross section, $\sigma_R = \tau G_M^2 + \varepsilon G_E^2$, is shown as a function of ε in Fig. 2. The uncertainties shown are the statistical and point-to-point systematic uncertainties. Additional corrections, *e.g.* the effect of a fixed angular offset for all points, would lead to a change in the cross sections that would vary approximately linearly with ε . These uncertainties would not contribute to the scatter of the points or deviations from linearity in the reduced cross section, but can modify the extracted value of the slope. These uncertainties are dominated by uncertainties in the ε dependence of the radiative corrections (0.3%), background subtraction, (0.25%), rate-dependent corrections in the tracking efficiency (0.25%), and the effect of a small beam energy or scattering angle offset (0.25%). These corrections yield a 0.55% uncertainty in the slope of the reduced cross section which is included in the uncertainties of the extracted form factors.

The form factors are obtained from a linear fit to the reduced cross sections. The results are given in Table II and the ratio $\mu_p G_E/G_M$ is shown in Fig. 3 together with the results of previous Rosenbluth and polarization transfer measurements. Note that for consistency with previous Rosenbluth measurements, the effects of Coulomb distortion [10] have not been included in the results in Table II. Correcting for Coulomb distortion would lower $\mu_p G_E/G_M$ by 0.048, 0.042, and 0.032 and increase $G_M/(\mu_p G_D)$ by 0.009, 0.007, and 0.006 for $Q^2=2.64, 3.2, \text{ and } 4.1 \text{ GeV}^2$, respectively.

TABLE II: Form factor values extracted from this measurement relative to the dipole form, $G_D = 1/(1 + Q^2/0.71)^2$.

Q^2	2.64 GeV ²	3.20 GeV ²	4.10 GeV ²
G_E/G_D	0.949 ± 0.040	1.007 ± 0.052	1.132 ± 0.077
$G_M/(\mu_p G_D)$	1.053 ± 0.015	1.048 ± 0.015	1.031 ± 0.015
$\mu_p G_E/G_M$	0.902 ± 0.038	0.961 ± 0.051	1.097 ± 0.077

The results presented here are in good agreement with form factors extracted from previous cross section data, but have much smaller statistical and systematic uncertainties. This fact, combined with the consistency of the various Rosenbluth measurements [4], rules out most explanations of the discrepancy in terms of possible experimental error in the cross section measurements. The accuracy of the present work leaves little room for doubting that the G_E/G_M ratios reported from the Jefferson Lab polarization transfer experiments are inconsistent with

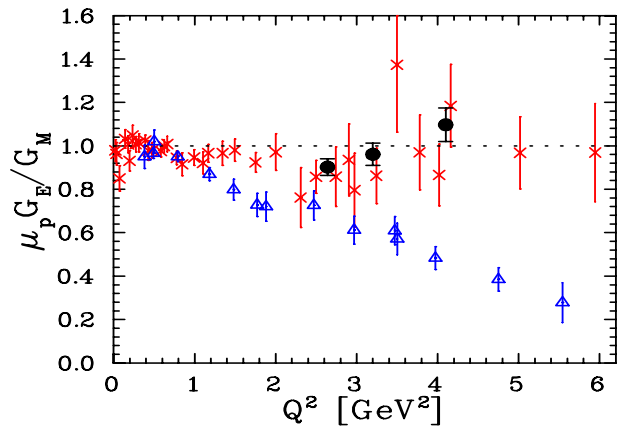


FIG. 3: (Color online) Extracted values of $\mu_p G_E/G_M$ from this work (circles), a global analysis of previous cross section data (Fig. 2 of Ref [9]) (crosses), and high- Q^2 polarization transfer measurements [5, 6] (triangles).

the form factors obtained using the Rosenbluth technique, and makes it clear that the problem is not simply experimental error in previous Rosenbluth measurements. The source of this discrepancy must be identified before the new insight into the proton structure provided by the recent polarization transfer data can be fully accepted.

One possible source for the difference between the two techniques is the effect of higher-order processes, or radiative corrections to the Born (one-photon exchange) cross section. The form factors are extracted from the cross section (or polarization transfer) measurements assuming the Born approximation, so the effects of additional processes must be removed from the measured cross sections. We correct the data for higher-order electromagnetic interactions such as bremsstrahlung, vertex corrections, and loop diagrams [8]. If we had detected the electron, the bremsstrahlung correction to the ε dependence of σ_R would have exceeded the ε dependence of G_E . In this experiment, the ε -dependent correction is much smaller and of the opposite sign. As the other radiative correction terms have almost no ε dependence, the consistency between the new data and previous Rosenbluth results provides a significant verification of the validity of the standard radiative correction procedures.

It has been suggested that higher-order processes such as two-photon exchange, not fully treated in standard radiative correction procedures, could explain the discrepancy [11, 12]. Such a correction would have to increase the cross section at large- ε by roughly 6% relative to the low- ε values. [9]. This would mean that the Rosenbluth form factors, the form factors extracted using only the cross section data, would have large errors due to these missing corrections. While two-photon exchange will also affect the polarization transfer data, the corrections to

the polarization transfer form factors are expected to be smaller, though not necessarily negligible [11, 13].

Additional experimental and theoretical effort is necessary to determine if the discrepancy in the form factor measurements can be explained entirely by higher-order radiative corrections. The effect of multiple soft photon exchange (Coulomb distortion) has been examined [10] and yields a change in the slope of 1–2%, corresponding to a 3–5% reduction in the extracted value of $\mu_p G_E/G_M$, well below the level necessary to explain the discrepancy. Recent calculations [12, 14] show significant corrections to the cross sections due to two-photon exchange, though they appear to explain only half of the observed discrepancy. Additional effort is going into calculations of two-photon exchange for the cross section and polarization transfer measurements. It remains to be seen whether the effects of two-photon exchange are the reason for what must otherwise be considered a severe discrepancy.

If missing radiative correction terms are responsible for the discrepancy, then the Rosenbluth form factors, and to a lesser extent the polarization transfer form factors, will not correspond to the true form factors of the proton. The discrepancy must be resolved before precise comparisons can be made between models of proton structure and the measured form factors. While the Rosenbluth data may not provide the true form factors of the proton, they still provide a useful parameterization of the electron-proton cross section, with the missing higher-order corrections absorbed into the extracted form factors. Thus, the Rosenbluth form factors do reproduce the observed cross sections and provide the best parameterization when elastic scattering is used to compare the normalization of different experiments, or when the elastic cross section is used as input to the analysis of experiments such as quasielastic $A(e, e'p)$ scattering [9, 15].

In conclusion, we have performed an improved Rosenbluth extraction of the proton electromagnetic form factors using detection of the struck proton rather than the scattered electron to decrease dramatically the uncertainty in the extraction. The results are as precise as recent polarization transfer measurements, but are in

agreement with previous Rosenbluth separations and inconsistent with high- Q^2 polarization transfer data. The precision of these new results rules out experimental error in the Rosenbluth results as the source of the discrepancy between the two techniques, and provides a stringent test of the radiative corrections that are currently used in elastic $e-p$ scattering. There are indications that this difference might come from two-photon exchange corrections, but we must better understand the discrepancy before precise knowledge of the proton form factors can be claimed.

We gratefully acknowledge the staff of Accelerator Division, the Hall A technical staff, and the members of the survey and cryotarget groups at Jefferson Lab for their efforts in making this experiment possible. This work was supported in part by DOE contract W-31-109-ENG-38, NSF grants 0099540 and PHY-00-98642, NSERC (Canada), and DOE contract DE-AC05-84ER40150, under which the Southeastern Universities Research Association operates the Thomas Jefferson National Accelerator Facility.

-
- [1] M. N. Rosenbluth, Phys. Rev. **79**, 615 (1950).
 - [2] R. C. Walker et al., Phys. Rev. D **49**, 5671 (1994).
 - [3] M. E. Christy et al., Phys. Rev. C **70**, 015206 (2004).
 - [4] J. Arrington, Phys. Rev. C **68**, 034325 (2003).
 - [5] M. K. Jones et al., Phys. Rev. Lett. **84**, 1398 (2000).
 - [6] O. Gayou et al., Phys. Rev. Lett. **88**, 092301 (2002).
 - [7] J. Alcorn et al., Nucl. Inst. & Meth. **A522**, 294 (2004).
 - [8] R. Ent et al., Phys. Rev. C **64**, 054610 (2001).
 - [9] J. Arrington, Phys. Rev. C **69**, 022201(R) (2004).
 - [10] J. Arrington and I. Sick, Phys. Rev. C **70**, 028203 (2004).
 - [11] P. A. M. Guichon and M. Vanderhaeghen, Phys. Rev. Lett. **91**, 142303 (2003).
 - [12] P. G. Blunden, W. Melnitchouk, and J. A. Tjon, Phys. Rev. Lett. **91**, 142304 (2003).
 - [13] J. Arrington (2004), hep-ph/0408261.
 - [14] Y. C. Chen, A. Afanasev, S. J. Brodsky, C. E. Carlson, and M. Vanderhaeghen (2004), hep-ph/0403058.
 - [15] D. Dutta et al., Phys. Rev. C **68**, 064603 (2003).